Environmental Earth Sciences (2019) 78:585
https://doi.org/10.1007/s12665-019-8596-2

ORIGINAL ARTICLE

Simulating the Xinmo landslide runout considering entrainment effect

Wei Liu[1,2,3] · Dongpo Wang[4] · Jiawen Zhou[5] · Siming He[1,2,3,6]

Received: 19 March 2019 / Accepted: 21 September 2019 / Published online: 28 September 2019

Abstract
This paper investigates the setting, causes, and main dynamic characteristics of the landslide that occurred at Xinmo village, Diexi, Sichuan province, China, on June 24, 2017. By comparing the pre- and post-sliding DEMs, the landslide involved the failure of $\approx 3.0 \times 10^6$ m^3 rock mass from its source area, and had a final volume of $\approx 6.3 \times 10^6$ m^3. The landslide runout extended 2800 m horizontally and 1200 m vertically, and covered an area of $\approx 143.1 \times 10^4$ m^2. Field investigation indicates that entrainment was one of the major causes of the increase in volume of landslide. To reproduce the behavior of the landslide runout, a depth-averaged continuum model that takes entrainment into consideration is applied. The simulated results generally agree well with the characteristics of the sliding path and distribution of the landslide deposit as observed in the field. It is demonstrated that entrainment plays a significant role in landslide mobility and volume. The final volume of the landslide is calculated about 6.21×10^6 m^3, which has more than double its initial volume.

Keywords Xinmo landslide · Runout · Entrainment · Numerical simulation · Dynamic analysis

Introduction

Landslides are one of the common geohazard worldwide. Some can cause huge economic losses and secondary disasters, under special conditions, because of their volume or mobility (Legros 2002; Pudasaini and Miller 2013). In recent years, global climate change and geological activities such as glacial recession and earthquakes have provided favorable conditions for the occurrence of catastrophic landslides (Yin et al. 2009; Allen et al. 2011; Tsou et al. 2011; Gariano and Guzzetti 2016). Therefore, it is necessary to improve risk assessment to prevent or mitigate the adverse impact of landslides.

To reduce the damage caused by catastrophic landslides, it is necessary to understand their mechanisms, including failure and movement. The former, for most of catastrophic landslides, is the result of the comprehensive functions of long- and short-term factors. Long-term factor, such as climate (Bovis and Jakob 1999), rock weathering (Regmi et al. 2013), and freeze–thaw cycles (Mateos et al. 2012), can slowly change the properties of a slope body. For example, the formation of the Sangrumba landslide that occurred in Nepal Himalaya was mainly influenced by rock weathering that drastically decreased the strength of the rock (Regmi et al. 2013). Compared to this, short-term factors such as earthquakes (Cui et al. 2009), heavy rainfall (Kim et al. 2012), and groundwater (Chigira et al. 2003) destroy the structure of slope body more quickly. For example, the Tsaoling landslide that occurred in Southwestern Taiwan was triggered by the 1999 Chi–Chi earthquake that resulted in several cracks being spread from the shear plane to ground surface (Chigira et al. 2003). Thus, triggering factors should be comprehensively considered to study the failure mechanism of a landslide. The latter, for most of catastrophic landslides, always has some remarkable characteristics such as high volume or mobility. High mobility of the catastrophic landslides could be caused by terrain conditions such as

✉ Siming He
hsm@imde.ac.cn

1 Key Laboratory of Mountain Hazards and Surface Process, Chinese Academy of Science, Chengdu, China

2 Institute of Mountain Hazards and Environment, Chinese Academy of Sciences, Chengdu 610041, China

3 University of Chinese Academy of Sciences, Beijing, China

4 National Laboratory of Geohazard Prevention and Geoenvironment Protection, Chengdu University of Technology, Chengdu, China

5 State Key Laboratory of Hydraulics and Mountain River Engineering, Sichuan University, Chengdu, China

6 CAS Center for Excellence in Tibetan Plateau Earth Sciences, Beijing, China

large differences in elevation or special conditions such as entrainment (Hungr and Evans 2004) and dynamic fragmentation of rock (Davies and McSaveney 2009). Therefore, the movement mechanisms should be studied carefully when conditions are different.

Recently, with the development of the computer technique, the prediction or back analysis of the dynamic processes of landslides even more important for risk assessment, as it provides data on characteristics such as sliding velocity and impact area. Several numerical models and computation methods have been proposed for the dynamic prediction and risk evaluation of landslides, based on their failure and movement mechanisms (Lourenço et al. 2006; Pastor et al. 2014; Savage and Hutter 1989). Each model and method has its own characteristics that reflect landslide processes by taking different factors into consideration, and has also reproduced the dynamic processes of landslides successfully by comparing numerical results with experimental data and field measurements. Most numerical models focus mainly on the properties of the landslide body and its influence on mobility by assuming a constant volume for the duration of motion. However, landslide paths are typically covered by loose surficial deposits such as colluvium, residual soil, and organics (McDougall and Hungr 2005). Entrained path material can influence the mobility or increase the volume of the landslide significantly (McDougall and Hungr 2005; Zhou et al. 2016). For example, the 1999 rock avalanche that occurred in Nomash River increased in volume from about 3.7×10^5 to 7.7×10^5 m^3 before reaching the valley floor by entrainment (Pirulli and Pastor 2012). Thus, the effect of entrainment that occurs during the sliding process is needed to be further considered.

In this paper, the geological conditions, causes, and main characteristics of the landslide that occurred at Xinmo village on June 24, 2017, in Sichuan, China, are summarized. According to the field investigation, the volume of landslide had a remarkable increase over the sliding process, and entrainment was considered to be the primary cause of it. To better understand how entrainment affects the behavior of the landslide runout, a depth-averaged continuum model taking entrainment into consideration and using the Coulomb friction law is applied. In addition, some influencing factors concerning entrainment are analyzed.

The Xinmo village landslide

On June 24, 2017, a catastrophic landslide (located at 32°04′9.4″N and 103°39′3.4″E) occurred at Xinmo village, Diexi town, in Sichuan province, southwest China (Fig. 1), causing 10 fatalities, leaving 73 missing, and burying 46 buildings. The landslide runout extended 2800 m horizontally and 1200 m vertically. This was equivalent to an effective friction angle of 24° and covered an area of $\approx 143.1\times10^4$ m^2. Based on a comparison of pre- and post-event digital elevation models (DEMs), the landslide

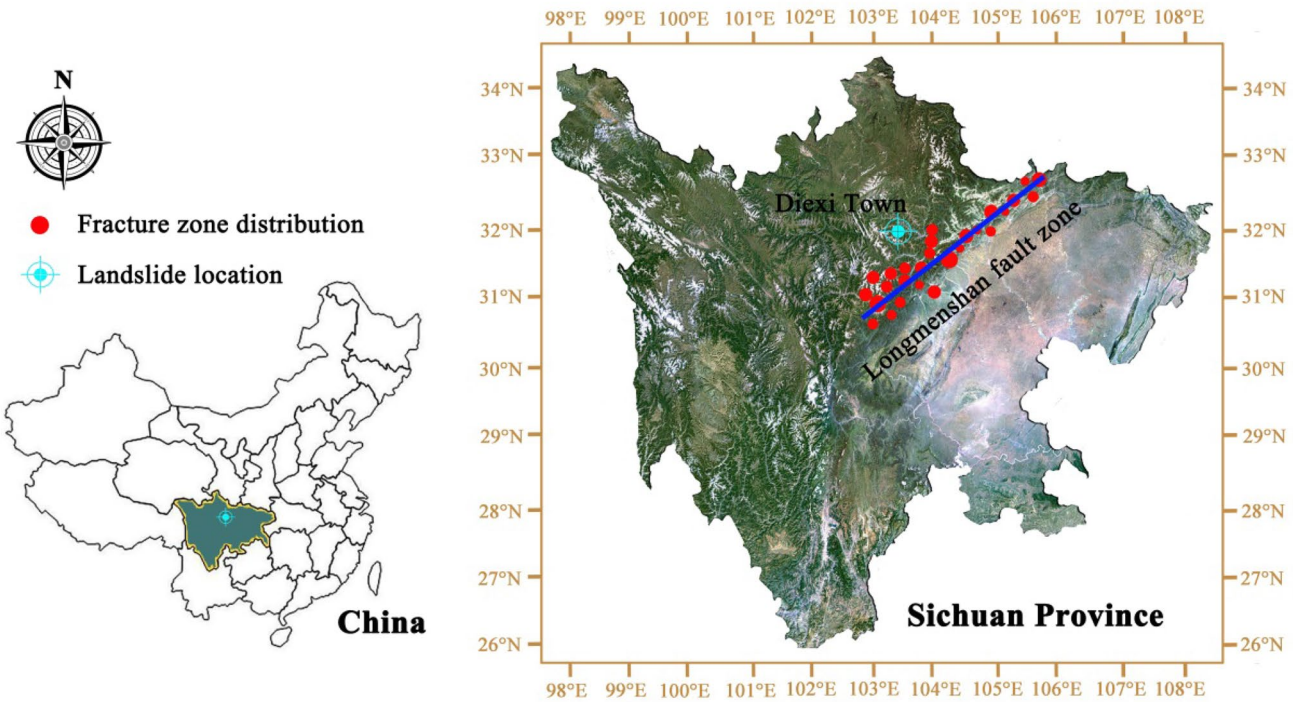

Fig. 1 Locations of the Xinmo village landslide and the distribution of the fracture zone

initially involved displaced material from the source area of 3×10^6 m^3 (Bai et al. 2019); however, with the effects of entrainment and rock fragmentation during transport, its final volume became $\approx 6.3 \times 10^6$ m^3 (Fan et al. 2017a, b). The duration of the landslide was about 100 s, according to records from Sichuan Seismic stations. Based on high-performance unmanned aerial vehicle (UAV) aerial photogrammetry, the sliding range of landslide was divided into three areas (see Fig. 2):

(a) Source area: the landslide source area contained steep terrain with a slope $\approx 53°$. The main body consisted of quartz sandstone. The rear and toe elevations of the landslide source area were 3428 m and 3328 m, respectively, giving a height difference of 100 m; the source area was an irregular trapezoid in profile, with a longitudinal length of 440 m and lateral width of 350 m. The slip direction of the landslide was mainly towards the southwest.

(b) Middle impact-shoveling area: this area, located between the leading edge of the source area and the old landslide accumulation area, has a longitudinal length of 1210 m and a lateral width of 367 m and a slope of 27°. Subjected to the narrow and straight terrain of the valley, the landslide slip direction was still mainly towards the southwest.

(c) Accumulation area: the terrain of this area was flat and wide, which made the landslide spread out during transport; the accumulation area had a lateral width of 1200 m and an area of $\approx 72 \times 10^4$ m^2. The average thickness of the deposit was approximately 8 m, although the local maximum thickness could exceed 30 m. The landslide destroyed houses, and impacted and blocked the Songpinggou River, a tributary of Minjiang River, and formed a 2000 m long dammed lake. A 2100 m section of the Township Road No. 104 was also buried, and the broken rock mass was observed clearly in this area. Moreover, the mud that splashed onto the other side of Songpinggou river, and areas, where the trees and shrubs collapsed on the outside edge of the accumulation area, were also seen clearly (Fig. 3). It indicates that the landslide moved at a high velocity.

Apart from these areas that were direct influenced by the landslide, there was an unstable slope at the west of the source and middle impact-shoveling areas (Fig. 2b). The rear of the unstable slope was 3350 m high. This potential hazard area was caused by the traction of the landslide, and divided into two parts by a 35 m wide tension crack (Fan

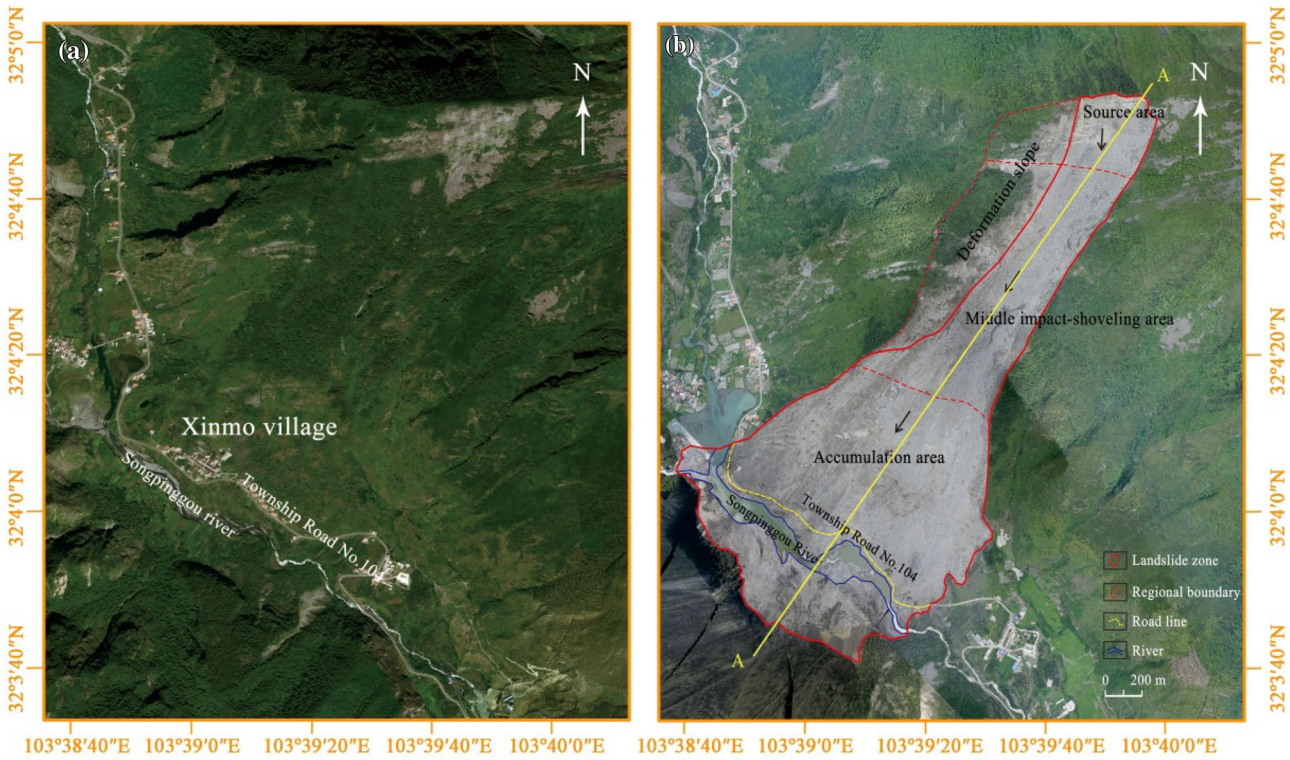

Fig. 2 Images showing catastrophic landslide at Xinmo village, Diexi town, Sichuan province, in southwest China. **a** Mountain slope before the landslide. **b** Same area after the landslide

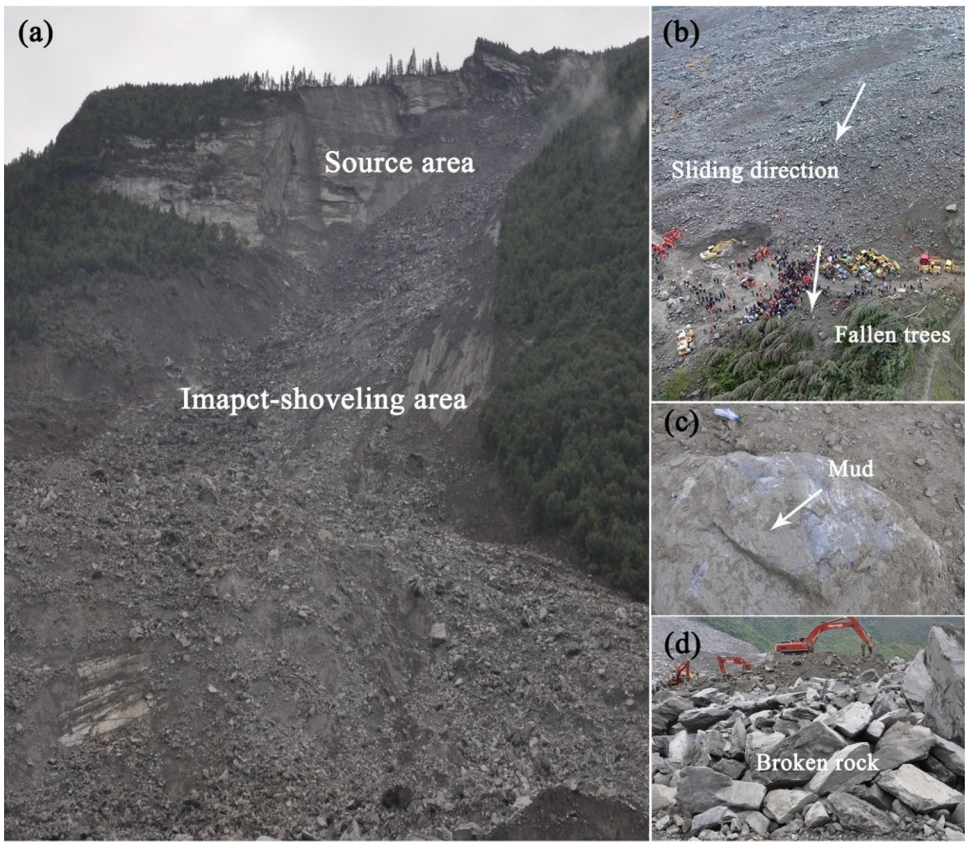

Fig. 3 Photos from the site: **a** close-up of the source and middle impact-shoveling areas; **b** fallen trees; **c** stone and mud; and **d** broken rock

et al. 2017a, b; Ouyang et al. 2017a, b). The leading edge of the unstable slope was wedge-shaped in profile and covered an area of $\approx 18.4 \times 10^4$ m^2. The rear edge of the unstable slope was an irregular diamond in profile, covered an area of $\approx 7 \times 10^4$ m^2, and consisted mainly of quartz sandstone bedrock.

Analysis of the cause of the landslide

Landslides generally occurred under certain conditions, such as great differences in elevation, heavy rainfall, and cracked geological structures (Khan et al. 2011; Rahman et al. 2014). From this point of view, the cause of the Xinmo village landslide is analyzed using a combination of these impact factors, a field investigation, and the three additional aspects. The first aspect is landform and topography. The landslide developed at the top of a sharp ridge line located at the left bank of the Songping river that belongs to a first-order tributary of the Minjiang river. This area has a rugged alpine terrain under the effect of strong tectonic erosion, and its strata outcropping belong to the Weiguanqun formation of the Devonian, Carboniferous and Lower Permian periods, and to the Zagunao and the Bocigou formations of thee Triassic (Fan et al. 2017a, b). Marbleized limestone, metamorphic sandstone, and phyllite are the main components of this area. For the Xinmo landslide, it developed within the Zagunao formation that consists of metamorphic sandstone interacted with slate. The mountainous region in which the Xinmo village landslide occurred is located in an NE–SW transition belt from the Chengdu Plain to the Qinghai–Tibet Plateau (Gao et al. 2017). The v-shaped valley has an elevation difference of over 1600 m. The geological cross section along profile line A–A (Fig. 2) was drawn based on field investigation, geological analysis, and interpretation of aerial images. Both sides of the mountain are steep and the slopes of the upper and middle parts of the mountain are greater than 50° (Fan et al. 2017a, b). These provide favorable energy conditions for the formation of landslides. The second additional aspect is the geological structure of the land. The landslide region is in the middle of the Longmenshan fault zone, where fold and fault structures are very developed. There are existed four arcuate faults, including Jiaochanggou Fault, Chahuagou Fault, Guancaigou Fault, and Shidaguan Fault. These arcuate faults are crossed slantwise by a North–West-trending fault (named Songpinggou Fault) that develops nearly along the Songping river. The Songpinggou Fault is originating from Moshi village and ending at Guanyinya near Jiaochang village, which plays a key role in triggering and controlling the development of geological hazards in this area (Wang et al. 2008). In this area, the rock stratum has an occurrence of 184°/53°, and

its trend is close to the main slip direction of the landslide. Moreover, this area is near the epicenter of the 7.5 M Diexi earthquake that occurred on March 25, 1933 (Chai et al. 1995); several landslides were induced afterwards (Wang et al. 2008). The combined effects of repeated earthquakes on this area after 1933, including the 2008 Wenchuan earthquake, exacerbated the slope and damage to the rock mass. The seismic intensity in the earthquake reached Level X, causing the mountain to crack (Chai et al. 1995). These are favorable geological structural conditions for landslide formation. The abundantly developed tension cracks and lateral fissures caused by historical earthquakes made the slope unstable. According to a Google Earth image from August 8, 2003, three macroscopic cracks can be found in the source area along the sliding direction of the landslide (Fig. 4). It suggests that the slope had been already gravitationally deformed and was prone to future failure long time ago (Fan et al. 2017a, b; Su et al. 2017). The third additional aspect is rainfall infiltration. The local climate is controlled by the monsoon climate of the East Tibetan Plateau, with a maximum recorded daily rainfall of 104.2 mm and an average annual precipitation of 716.5 mm (Wang et al. 2008). There was more rainfall in Maoxian province during the 2017 flood season than in the previous years. According to records from two rainfall observation stations near Diexi, the cumulative rainfall exceeded 200 mm from May 1 to June 23 (Fig. 5). After continuous rainfall from June 8 to 14, there was a 42% increase in monthly rainfall compared to the same period in the previous years. The stability of the rock slope was thus reduced gradually with the continuous rainwater seepage, adding further to the conditions that resulted in the landslide (Ouyang et al. 2017a, b).

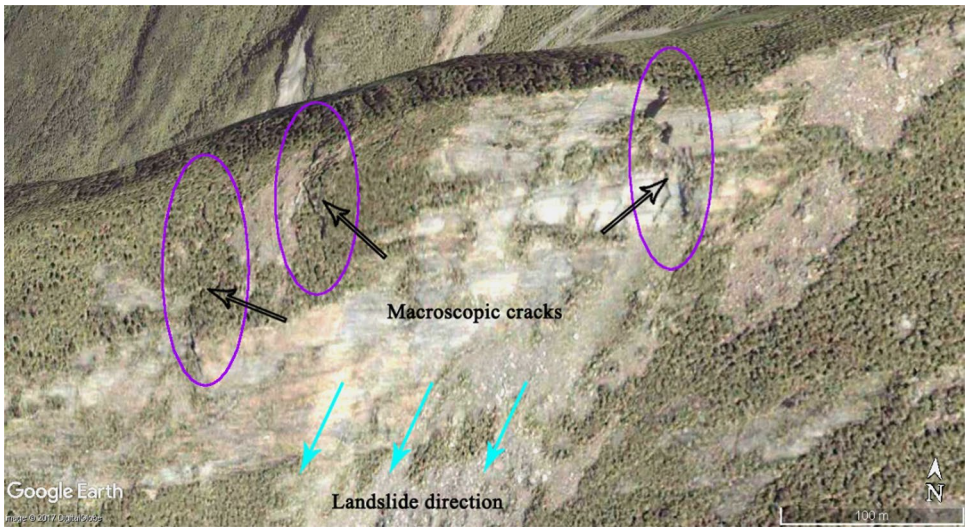

Fig. 4 Google Earth image from August 8, 2003, showing that macroscopic cracks existed in the source area before the Xinmo village landslide

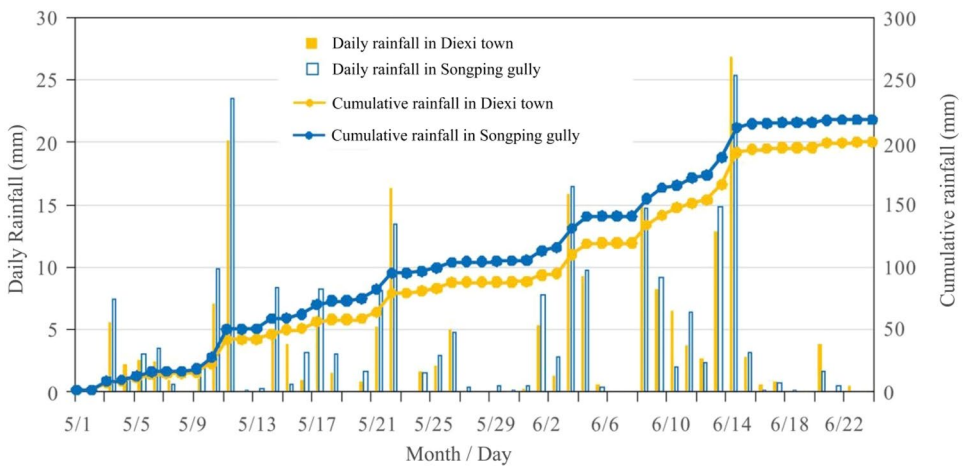

Fig. 5 Daily and cumulative rainfall from May 1 to June 23, 2017, recorded at rainfall observation stations near Xinmo village

Analysis of the entrainment process of the landslide

Entrainment, as a remarkable feature of the Xinmo landslide, is a continuous process along with the movement of the landslide. Meanwhile, its influence to the landslide is dynamic. Thus, having the knowledge of the evolution of entrainment is necessary, for analyzing the effect of entrainment on the landslide. In this study, based on the field investigations and remote-sensing techniques, three stages of the entrainment process were presented as follows (Fig. 6):

(a) The main block with a volume of 3×10^6 m^3 ruptured suddenly at the source area, and impacted the surface of valley (Fig. 3a). Then, the block transformed into relatively small particles and then shoveled some of the surface materials, which makes the sliding mass having some fluidization characteristics (Su et al. 2017). This change is more conductive to the occurrence of entrainment. However, the entrainment-induced change on the velocity and volume of landslide is small at this stage.

(b) After that, the mass slid along the high slope, and its characteristics change in the aspect of velocity and volume. A large volume of unconsolidated substrate materials was scraped in the middle area and mixed with the sliding mass, which have a strong effect on the flow characteristics of the landslide. In this stage, the velocity and volume of the landslide increased significantly under the combined effect of continuous entrainment and gravity (Fan et al. 2017a, b; Ouyang et al. 2017a, b). Meanwhile, the shear force from landslide on eroded bed surface also became larger, which means that the erosion ability of the landslide reached maximum. According to the thickness distribution obtained from the difference between the DEM pre- and post-events, a mass of about 3.3×10^6 m^3 was eroded by the sliding mass, whereas the averaged thickness of the eroded layer was about 10 m.

(c) Finally, the sliding mass with large volume and high velocity entered the flat area, and spread not only to downstream, but also to either side. Then, its velocity decreased quickly due to the increase of frictional resistance, which leads to little surface materials scraped. The thickness of deposits at the Xinmo village was about 5–10 m, with a maximum value of 15 m. For the deposits along the river, its averaged thickness was 10–15 m with a local maximum value of over 20 m.

Description of models

To investigate the behavior of the runout of the Xinmo village landslide, a depth-averaged model was used to study its dynamics (Hungr and McDougall 2009; Gray and Edwards 2014). This model reduces the complicated three-dimensional Navier–Stokes equations into a simple two-dimensional continuum problem by neglecting the changes in the vertical motion characteristics of the landslide, which depends on its large aspect ratio; in other words, if its lateral extension was large compared to the thickness of the layer (Pitman et al. 2003; Savage and Hutter 1989). This greatly decreases the computation cost while preserving information on the fundamental behavior of landslide, and has been validated by a series of experimental benchmarks and real hazards (Liu et al. 2016; Ouyang et al. 2015, 2017a, b). Besides, this model also assumes that the landslide consists of homogeneous material and has a large deformation by neglecting its complex material component. This hypothesize could capture the flow characteristics of landslide well while considering the effect of material properties on landslide motion, e.g., anisotropy. Moreover, entrainment was considered as one of the main factors that increased the volume of the Xinmo village landslide, and the effect of entrainment is considered in the applied model. It is assumed that the eroded materials could mix well with the landslide and its properties are the same with that of the landslide, which is helpful for highlight the effect of entrainment on landslide motion while neglecting some extra special phenomena, e.g., dilatancy. A traditional Cartesian coordinate system, *O-xyz*, is introduced; the *x*-axis is along the horizontal direction, the *y*-axis lies in the cross direction, and the *z*-axis is parallel to the direction of the gravitational acceleration (Chen and Lee 2003). Using this coordinate system, detailed topographic effects can be included in the gradients of the basal topography in the *x*- and *y*-directions (Fischer et al. 2012). According to Pitman et al. (2003), the governing equations, based on the conservation of mass and momentum, can be expressed as

$$\partial_t h + \partial_x(hu) + \partial_y(hv) = E, \tag{1}$$

$$\partial_t(hu) + \partial_x\left(hu^2 + \frac{1}{2}k_x g_x h^2\right) + \partial_y(huv) = u_b E + g_x h - \frac{u}{|\mathbf{u}|}\mu g_z h, \tag{2}$$

$$\partial_t(hv) + \partial_x(huv) + \partial_y\left(hv^2 + \frac{1}{2}k_y g_y h^2\right) = v_b E + g_y h - \frac{v}{|\mathbf{u}|}\mu g_z h, \tag{3}$$

where t is time; h is the thickness of the landslide; $\mathbf{g}=(g_x, g_y, g_z)$ is gravitational acceleration; $\mathbf{u}=(u, v)$ denotes the velocity components in the x- and y-directions, and $\mathbf{u}_b=(u_b, v_b)$ is the velocity at the lower boundary corresponding to each velocity component (Pitman et al. 2003; Iverson and

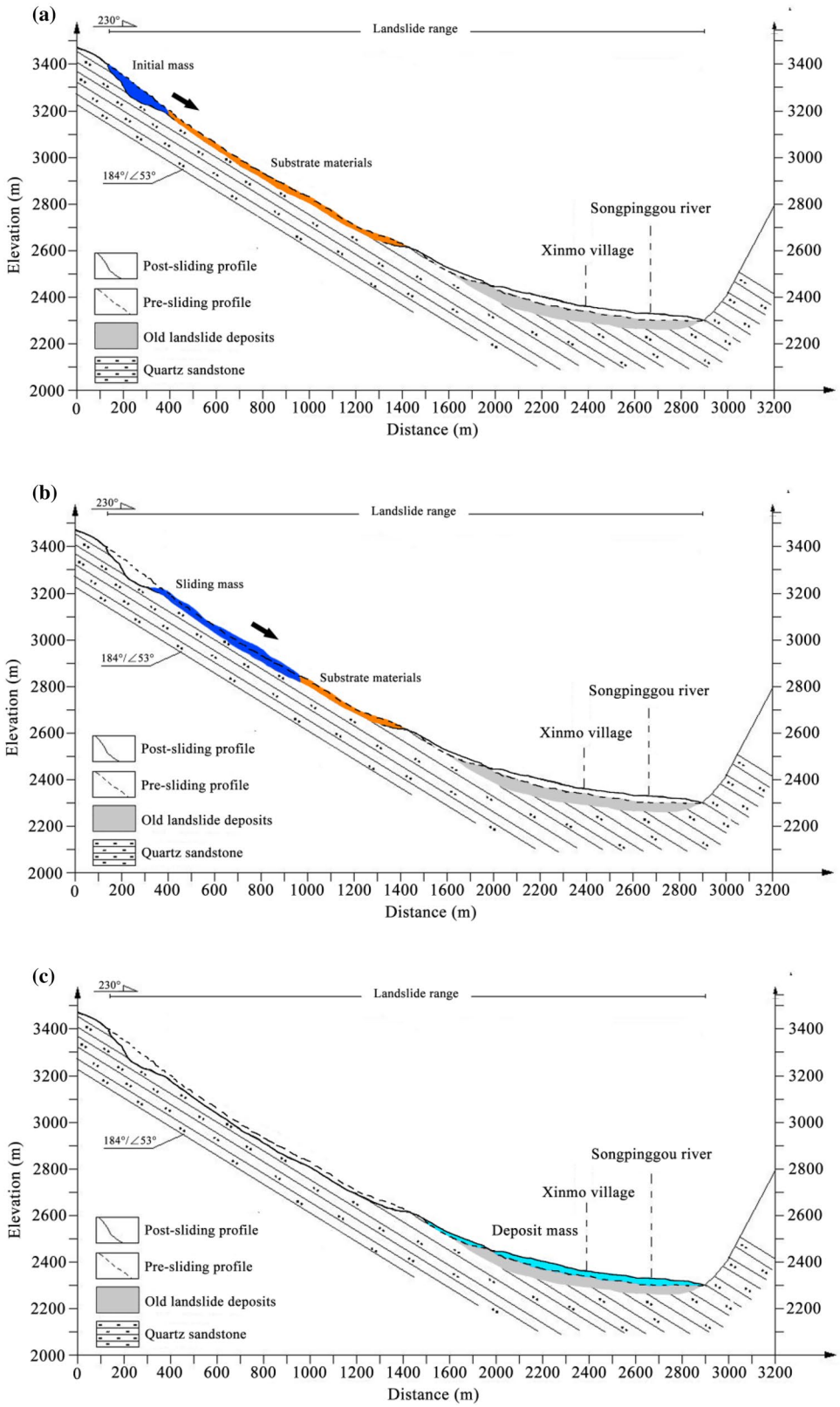

Fig. 6 Sketches of the entrainment processes of the landslide

Ouyang 2015); $\mu = \tan\varphi_{bed}$ represents the friction coefficient of the rock avalanches in contact with the bed, where φ_{bed} is the basal friction angle; E is the basal entrainment rate; and $\mathbf{k} = (k_x, k_y)$ represents the lateral stress coefficient in the x- and y-directions. Depending on whether the material being studied is expanding or contracting, $k_{(x,y)}$ can be

defined using a function of the internal and basal angles. From a Mohr diagram, the formula for $k_{(x,y)}$ can be derived as follows (Savage and Hutter 1989):

$$k_x = \begin{cases} k_{x_{\text{act}}} & \partial u/\partial x > 0 \\ k_{x_{\text{pas}}} & \partial u/\partial x < 0 \end{cases}; \quad k_y = \begin{cases} k_{y_{\text{act}}}^{x_{\text{act}}} & \partial u/\partial x > 0,\ \partial v/\partial y > 0 \\ k_{y_{\text{act}}}^{x_{\text{pas}}} & \partial u/\partial x < 0,\ \partial v/\partial y > 0 \\ k_{y_{\text{pas}}}^{x_{\text{act}}} & \partial u/\partial x > 0,\ \partial v/\partial y < 0 \\ k_{y_{\text{pas}}}^{x_{\text{pas}}} & \partial u/\partial x < 0,\ \partial v/\partial y < 0 \end{cases}, \tag{4}$$

where $k_{x_{\text{act/pas}}}$ and $k_{y_{\text{act/pas}}}$ denote the lateral stress state in the x- and y-directions, respectively, and can be defined as a function of the internal and basal angles of friction:

$$\begin{cases} k_{x_{\text{act/pas}}} = 2\sec^2\varphi_{\text{int}}\left(1 \mp \left\{1 - \cos^2\varphi_{\text{int}}\sec^2\varphi_{\text{bed}}\right\}^{1/2}\right) - 1 \\ k_{y_{\text{act/pas}}} = \dfrac{1}{2}\left(k_x + 1 \mp \left\{\left(k_x - 1\right)^2 + 4\tan^2\varphi_{\text{bed}}\right\}^{1/2}\right) \end{cases}, \tag{5}$$

where "−" and "+" correspond to an active state and a passive state, respectively; φ_{int} is the internal friction angle of the landslide.

Entrainment, a phenomenon that frequently occurs on landslides in fields, may have a remarkable impact on the landslide mobility (Pirulli and Pastor 2012; Cuomo et al. 2016). Erosion action can also increase the volume of a landslide, and the volume of deposited material may increase several times with respect to the initial sliding mass (McDougall and Hungr 2005). This study investigates the effect of entrainment on landslide mobility while ignoring rock fragmentation. Since the importance of entrainment was realized, many formulas for entrainment rate have been proposed in the literature and greatly improved our understanding of this phenomenon (Blanc et al. 2011; Iverson and Ouyang 2015; Pudasaini and Fischer 2016). For entrainment, its extent relates to landslide movement, material properties and topographic feature (Cuomo et al. 2016; Hungr and Evans 2004). To consider these factors comprehensively and simply, the entrainment law proposed by Blanc et al. (2011), based on the analysis of data from experiments, is applied here as follows:

$$E = h \cdot |\mathbf{u}| \cdot K \cdot (\tan\theta)^{2.5}, \tag{6}$$

where θ is the slope angle; $|\mathbf{u}|$ is the modulus of vector $\mathbf{u}$, $|\mathbf{u}| = (u^2 + v^2)^{0.5}$; and K is an empirical parameter to be calibrated, and relates to the properties of landslide and bed materials.

Numerical implementation

The proposed numerical schemes employ a finite-volume method to discretize the model equations and a Riemann approximation solver to manage the discontinuous problem at the grid cell interface (Loukili and Soulaïmani 2007). However, there are two challenges to solving this system. First, it is important to preserve a steady state at the discrete level by balancing the flux and source terms. To satisfy this condition, several well-balanced schemes have been proposed (Gosse 2000). We refer to Audusse et al. (2004); this well-balanced scheme can also satisfy some natural properties such as non-negativity of flow depth and discrete entropy inequality. Second, spurious flow is always induced for complex terrain, especially at the wet or dry fronts (Bollermann et al. 2013). To manage this complexity, the local bed slope and variables such as flow depth and velocity need to be modified to prevent a non-physical flux across the grid cell interface. More details of this modification are described in Liang and Borthwick (2009).

Numerical analysis of the catastrophic 2017 landslide at Xinmo village, Diexi, Sichuan province, china

To accurately simulate the movement of a landslide, it is necessary to ensure that the elevation data used are close to that of the actual terrain. To achieve this, pre- and post-event DEMs from 2013 and 2017, respectively, were used to obtain the surface and subsurface geometry of the landslide accumulation. These terrain elevation data were provided by the Sichuan Geomatics Center at a spatial resolution of 5 × 5 m. The total initial volume in the calculation is 3.09×10^6 m^3. After the mobility indices for the landslide are quantified, the data can be used to evaluate its behavior and compare the simulated results with measured data. For the Xinmo village landslide, the basal frictional angle φ_{bed} is the most important parameter that influences the landslide mobility, and the value of this parameter can be estimated roughly using the ratio of vertical descent H and horizontal extent L (Iverson and George 2015; Ouyang et al. 2017a, b), $H/L = 0.42$, representing a friction angle of 24°. Another mobility index that affects landslide-spreading behavior is the normal stress coefficient k_{ap}. Equation (4) shows that determining this index requires the value of the internal friction angle φ_{int}. Field investigation indicated that the material source for the landslide consisted mainly of quartz sandstone; therefore, a common value of 35° is used for φ_{int} (Ouyang et al. 2017a, b). This is reasonable, even if it is somewhat greater than the friction angle for soil material. The entrainment parameter K is also a key parameter related to the material properties of the landslide and the eroded surface. Based on some characteristics (such as landslide runout, degree of erosion of the sliding zone, and distribution of accumulation) of the landslide event, the value of K is assumed to be 0.0018 after lots of calibrations. Actually, these characteristics of the event are both influenced by the properties of landslide and bed

materials such as saturated unit weight and dry-saturated weight. However, due to the limitation of the used model and the lack of field data, we have to use the value of K to reflect indirectly the effect of these material properties. A refined model for better incorporating the effects of theses material properties is needed to be investigated in future study. The empirical parameter value of $g = 9.8$ m/s^2 is also used to calculate landslide motion. Following Pudasaini and Fischer (2016), this case assumes that $\mathbf{u}_b$ is approximated by the averaged velocity, $\mathbf{u}_b = 0.5\mathbf{u}$.

The results of the simulation of the moving flow depth of the Xinmo landslide, and the corresponding erosion depth of the basal surface at different times $t = 0$, 20, 40, and 100 s, are shown in Figs. 7 and 8, respectively. The landslide and erosion of basal surface are outlined with colors representing different thicknesses. The maximum depth of the initial landslide in the source area is 81.3 m. Initially, the landslide accelerated due to the steep inclination of the slope after it collapsed. When the moving mass passed through the narrow section of the creek, the simulated mass reached a maximum velocity of 55 m/s. The simulation found that the erosion degree of the basal surface is highest in this area and that this was caused by the continuous movement and high velocity of the mass. After the terrain at the lower section of the creek was flattened and broadened, the moving mass decelerated and became a deposit under the effects of friction resistance. With the relatively flat terrain and the decreasing movement velocity, the degree of erosion

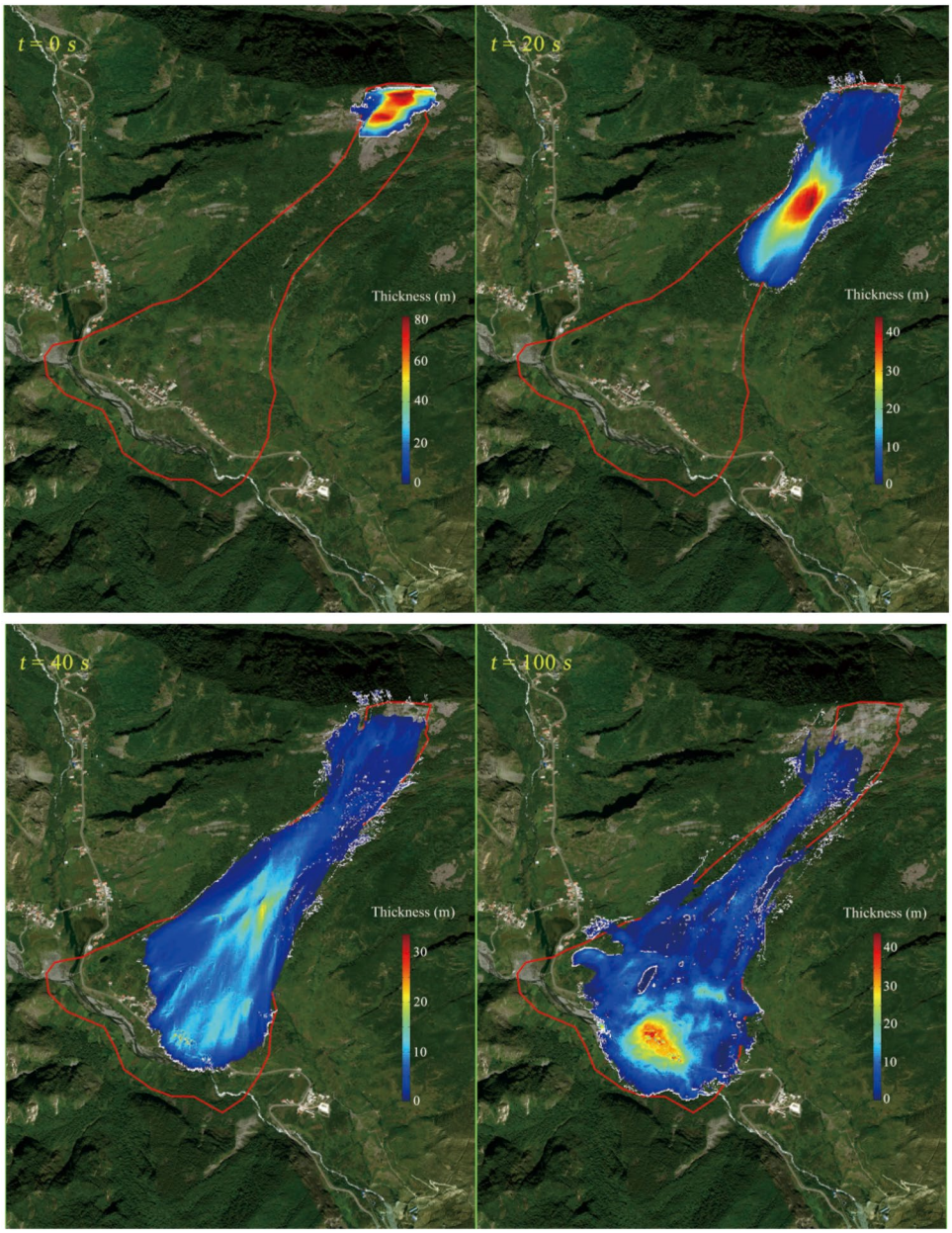

Fig. 7 Map views of the simulated behavior of the Xinmo village landslide. The red line is the outline of the landslide path; the background image is pre-event satellite imagery

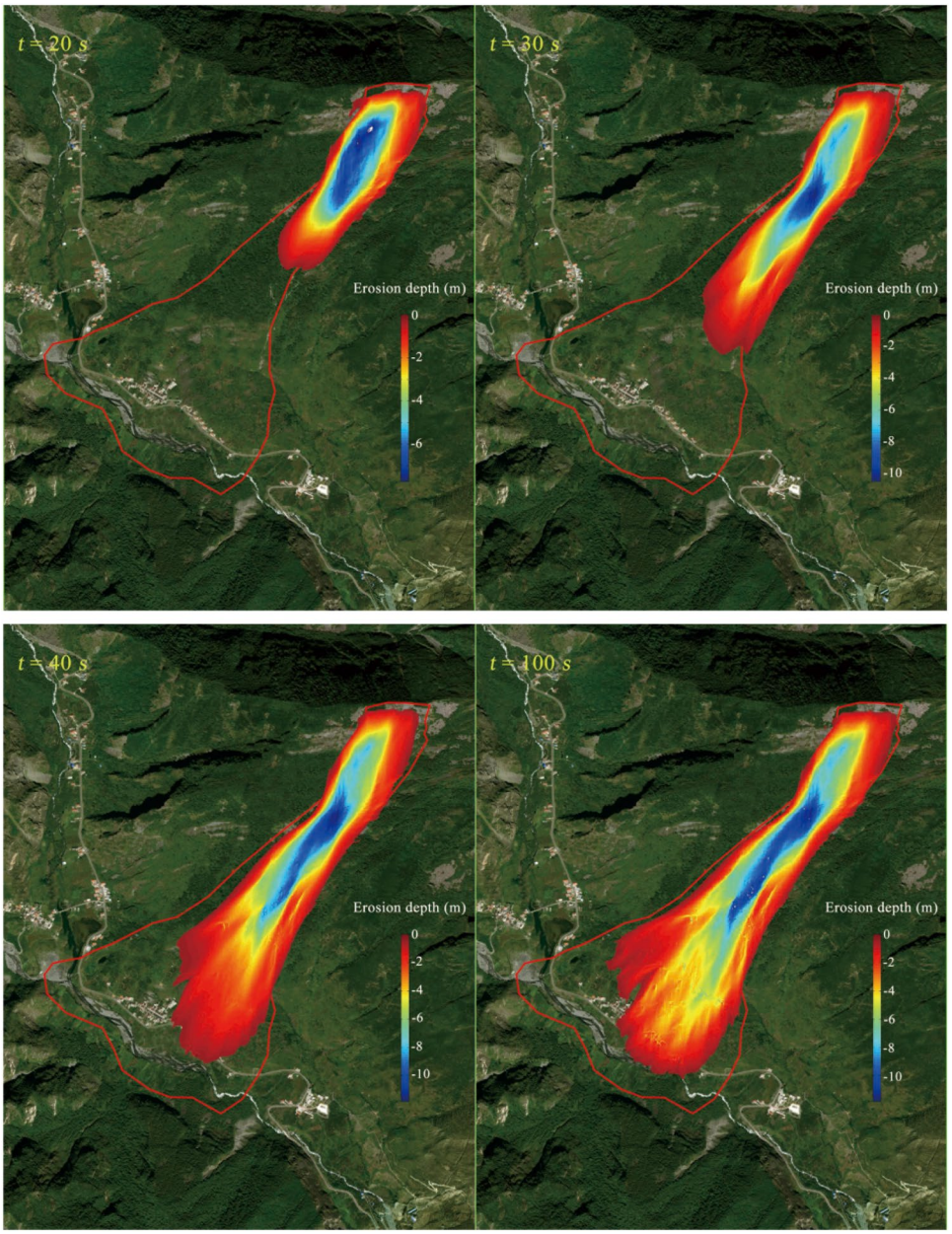

Fig. 8 Map views of the simulated erosion depth of the basal surface. The red line is the outline of the landslide path; the background image is pre-event satellite imagery

of the basal surface in this area decreases, even vanishing on the edge of accumulation area, where the moving velocity of mass is close to zero. Finally, the moving mass that destroyed Xinmo village and blocked the Songpinggou river had a maximum thickness of 45 m. The volume of the mass deposited downstream was computed as about 6.21×10^6 m^3, compared to the estimated volume of 6.3×10^6 m^3. Figure 8b shows that the computed deposit area of the landslide match well with data from the field investigation. The maximum eroded depth of the bed surface was computed as about 11.6 m, which as well as its location also match well with data from the field investigation (Fan et al. 2017a, b). However, there is a difference between computational flow area and measured sliding path at the western edge of the accumulation area. This could be attributed to field observations that show a hump in the middle of the accumulation area (Fig. 9a) (Yin et al. 2017). The moving mass impacted this hump during transport, and the part of this mass with a high velocity and low weight splashed westwards. However, this splashed material is only a small portion of total moving mass, and the average depth of the deposits on the western edge of the accumulation area are only about 2 m (as shown in Fig. 9b). Unfortunately, it is difficult for the depth-averaged continuum model to consider the splash behavior of a moving mass, and this is neglected in the current simulation. Nevertheless, the simulated results can provide a basis for risk evaluation and selecting sites for buildings.

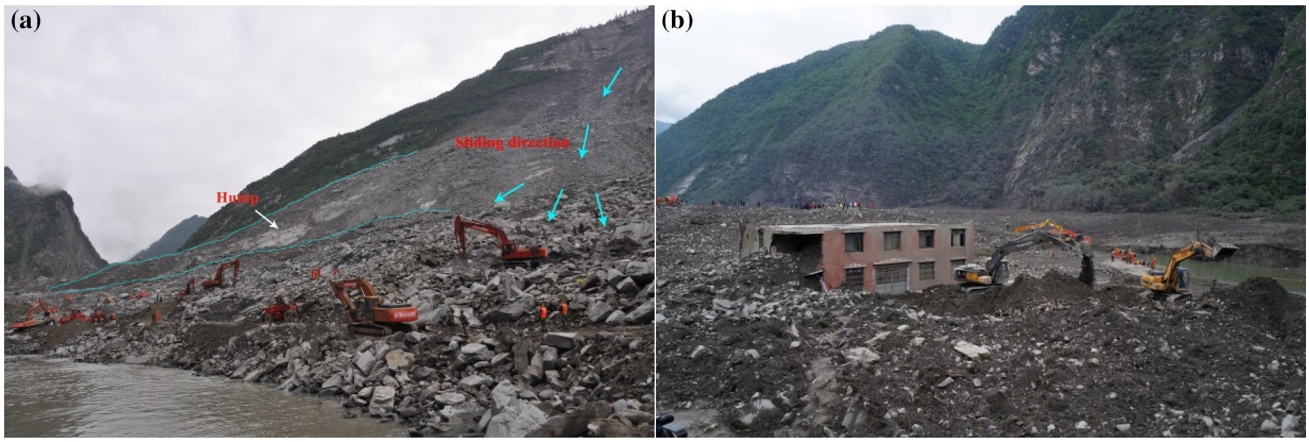

Fig. 9 **a** Hump located in the middle of the accumulation area. The blue lines indicate the sliding direction of moving mass and the blue line indicates the lower and upper boundaries of hump. **b** Western edge of the accumulation area

In addition, the effect of entrainment on landslide mobility was also investigated. The final deposited depths at $t = 100$ s, with and without entrainment, are shown in Fig. 10. Without entrainment, the travel distance and area influenced by the landslide are smaller, and the deposit is shallower, than when entrainment occurs. To illustrate the difference between the mobility of the landslide in the two cases, the evolutions of the maximum velocity and kinetic energy of the landslide during its run, are shown in Fig. 11. The simulation results show similar characteristics overall. Initially, the maximum velocity and kinetic energy of the landslide in the two cases are the same, because in the

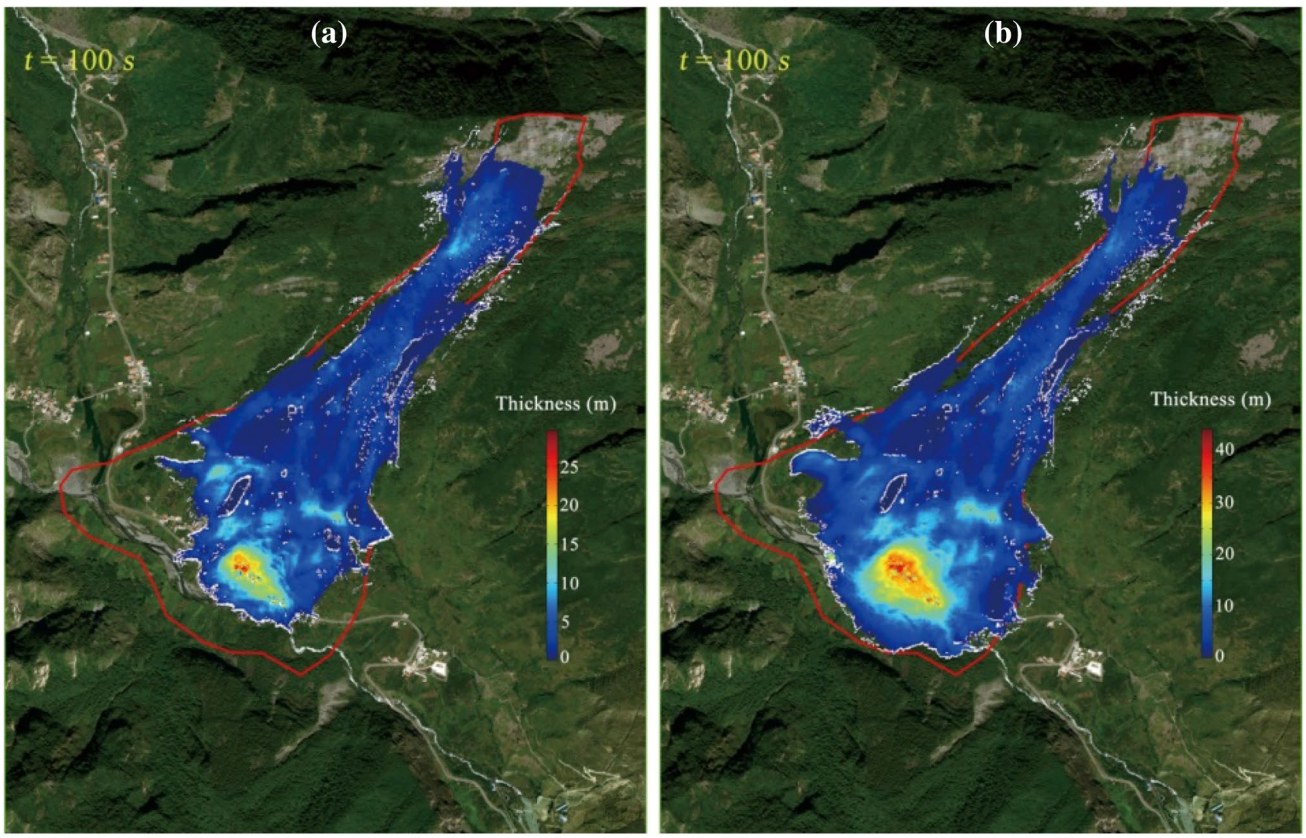

Fig. 10 Comparison of the simulated results between deposit distributions at $t = 100$ s, **a** without entrainment and **b** with entrainment

detaching area, the entrainment effect is absent. The maximum velocity with entrainment is smaller than without entrainment at an early stage, and becomes larger at a later stage. This is because that the sliding mass mixed with a large volume of unconsolidated substrate materials and the velocity is decreased based on the law of momentum conservation. Nevertheless, the eroded material gained kinetic energy from the sliding mass, and its kinetic energy went up with time under the gravity effect. In addition, because of that the total kinetic energy with entrainment is larger than without entrainment. When the sliding mass entered the flat area, its large kinetic energy resulted in a longer travel distance and larger influenced area. Moreover, it should be noted that the differences between the maximum velocity and kinetic energy of the landslide in the two cases are small when the entrainment is small. These differences become larger, since the effect of entrainment becomes more obvious. All of them show that entrainment can affect not only the volume of a landslide but also its mobility.

Discussion

Landslide mobility in alternative scenarios

Since the Xinmo landslide has been widely studied by several scholars that focus on investigating the geometrical feature (Fan et al. 2017a, b; Yin et al. 2017), triggering mechanism (Fan et al. 2017a, b; Su et al. 2017), and motion process (Chen and Wu 2018; Ouyang et al. 2017a, b), its characteristics at each stage were well summarized. These studies also agreed that entrainment is a main factor to influence the geometrical feature and motion process of Xinmo landslide, but the study on how this factor affects the landslide is still missing. Although Ouyang et al. (2017a, b) and Chen and Wu (2018) simulated the Xinmo landslide using different numerical approach, they both treated the eroded substrate materials as part of the initial mass of landslide. Entrainment is an ongoing process, which changes the movement features of

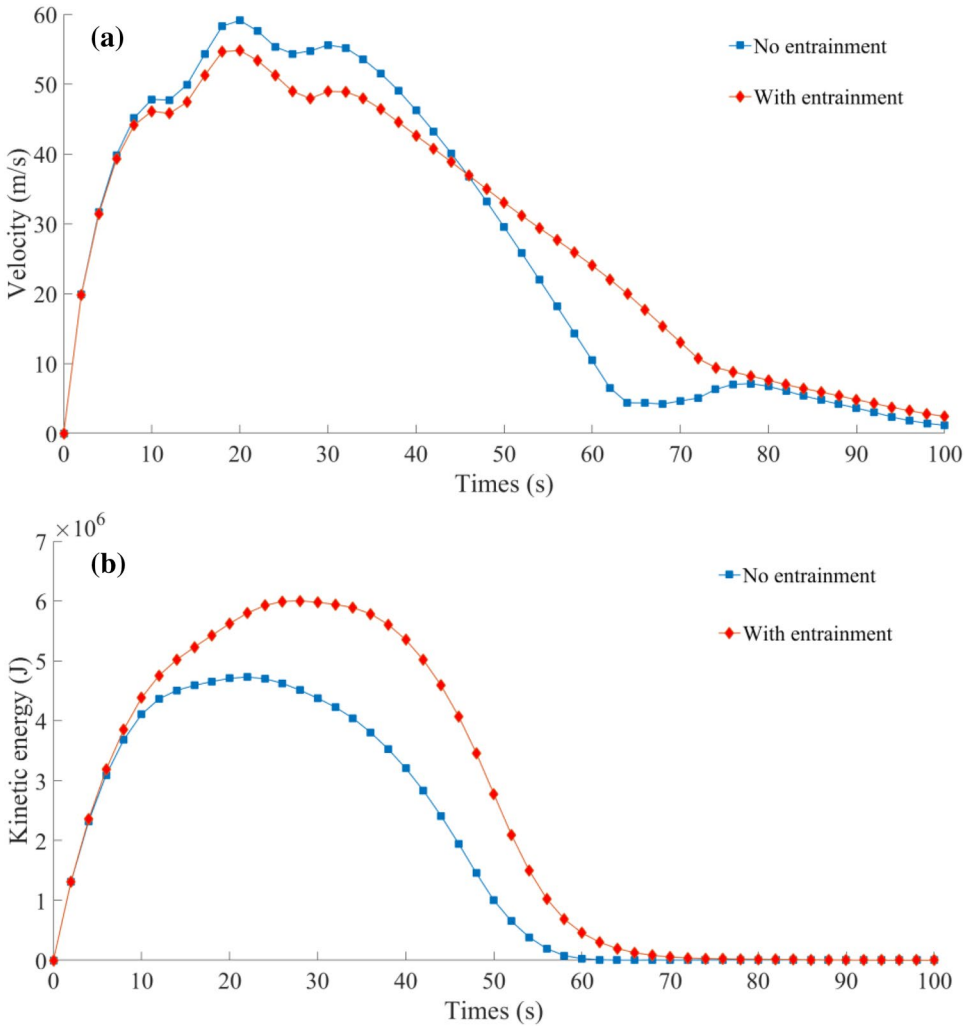

Fig. 11 Evolutions of maximum velocity and total kinetic energy of the Xinmo landslide in simulations with and without entrainment

landslide gradually. From this point of view, this study is the first discussion about the available motion scenarios using two initial settings and improves the knowledge of the dynamic process of the Xinmo landslide. Initial setting 1 is the same with Fig. 7 ($t = 0$ s), and initial setting 2 that has a landslide volume of 5.75×10^6 m^3 is shown in Fig. 12a. Both of these settings have the same parameters. The evolutions of the maximum velocity and kinetic energy of the landslide for two cases are shown in Fig. 13. The simulation results show that the velocity with setting 2 is smaller than with setting 1 at an early stage, and becomes larger at a later stage. Meanwhile, the maximum value of velocity with setting 2 is larger than with setting 1, and the time of it appearing is later. It is because that the eroded materials and source mass slid at the same time, which makes that the sliding mass has a larger kinetic energy from the start (Fig. 13b) and affects the movement of the landslide. The final shape of the landslide with setting 2 also has a great difference from the field investigation (Fig. 12b). These results indicate that it may be not appropriate to treat the eroded materials as part of the initial mass of landslide when simulating landslide movement.

Landslide velocity profiles for alternative scenarios

As suggested by Pitman et al. (2003) and Pudasaini and Fischer (2016), once the materials at the bottom have just been eroded, its velocities $\mathbf{u}_b$ are different than the depth-averaged (mean) velocities $\mathbf{u}$ that appear in the inertial (or, the convective) part. In addition, the value of $\mathbf{u}_b$ depends on the type of landslide velocity profile. However, it is difficult to determine the velocity profile within the part of a real landslide case, and the choice of a realistic velocity profile will be driven by several considerations. Here, the values of $\mathbf{u}_b$ ranging from $0.2\mathbf{u}$ to $0.8\mathbf{u}$ corresponding to different velocity profiles are used for simulation, to study its influence on landslide mobility. Clear trends emerge when mobility indices of landslide are calculated from the results of alternative simulations that use different values of $\mathbf{u}_b$ (Fig. 14). The velocity and total kinetic energy of the landslide are both enhanced when a larger value of $\mathbf{u}_b$ is applied. For these three cases ($\mathbf{u}_b = 0.2\mathbf{u}$, $0.5\mathbf{u}$, $0.8\mathbf{u}$), the final volumes of landslide are 5.95×10^6 m^3, 6.21×10^6 m^3, and 6.43×10^6 m^3, respectively. It indicates that the mobility and entrainment ability of the landslide are interacted on each other. Once entrainment occurs, it enhances the landslide mobility and further leads to more eroded substrate materials. However,

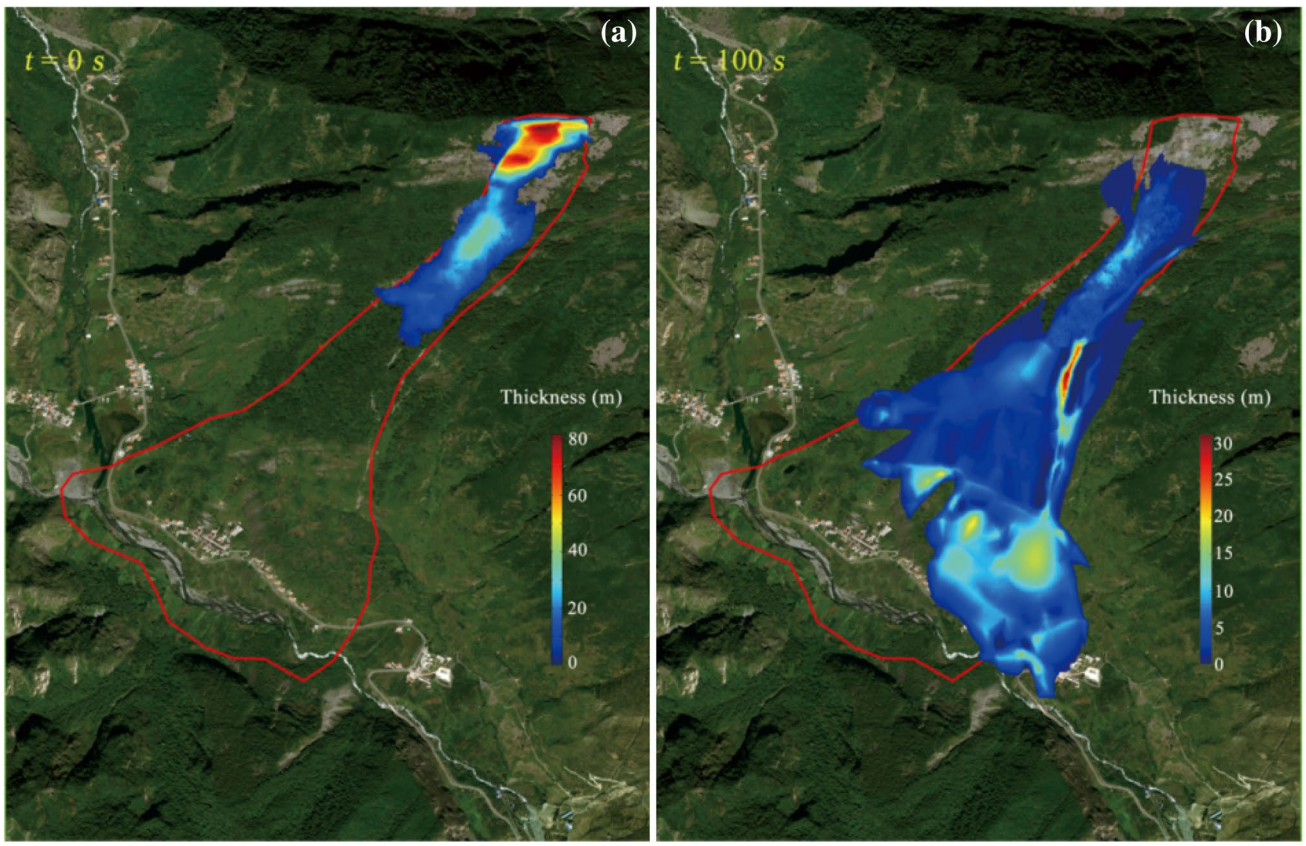

Fig. 12 Initial and final shape of the landslide for the case with setting 2

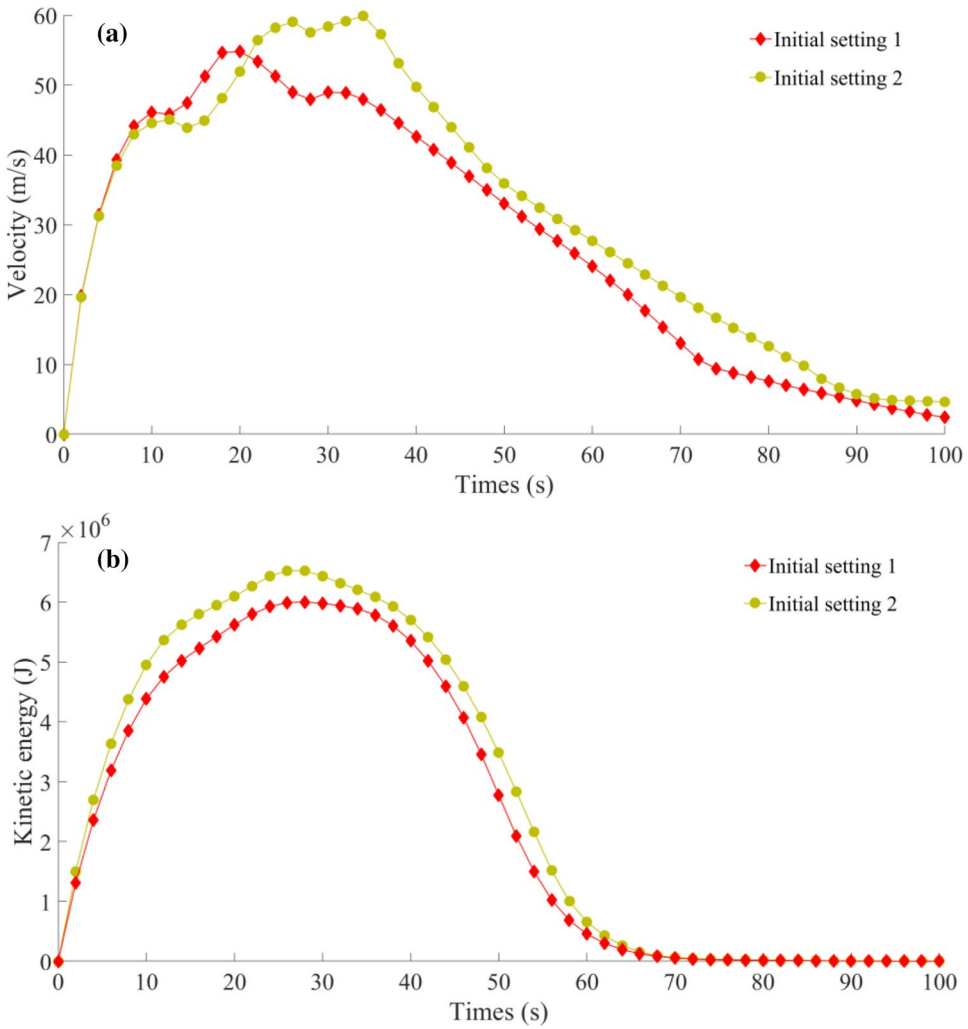

Fig. 13 Evolutions of maximum velocity and total kinetic energy of the landslide in simulations with two settings

this behavior will only be experienced on steep terrain which provides favorable conditions for eroded material to gain kinetic energy under the gravity effect. If the sliding mass entry a flat area, the eroded materials cannot gain enough kinetic energy and, therefore, decrease the mobility of sliding mass due to the law of momentum conservation.

Conclusion

On June 24, 2017, a catastrophic landslide occurred at Xinmo village, Diexi town, in Sichuan province, China. This paper investigated the general setting, causes, and main dynamic characteristics of the landslide. Based on field investigations, entrainment is considered as one of the major causes of the increase in volume of landslide. The dynamic process of the landslide is reproduced and analyzed using a depth-averaged continuum model. The results from the simulation are compared with field observations and measurements; these indicate that the depth-averaged continuum model is able to capture the runout behavior of the landslide well by considering the effect of entrainment. The effects of entrainment on landslide mobility were also investigated, and results show that entrainments enhance the latter. These results suggest that a depth-averaged continuum model that considers special conditions can be used to predict similar types of landslides and assist in risk evaluation and building site selection.

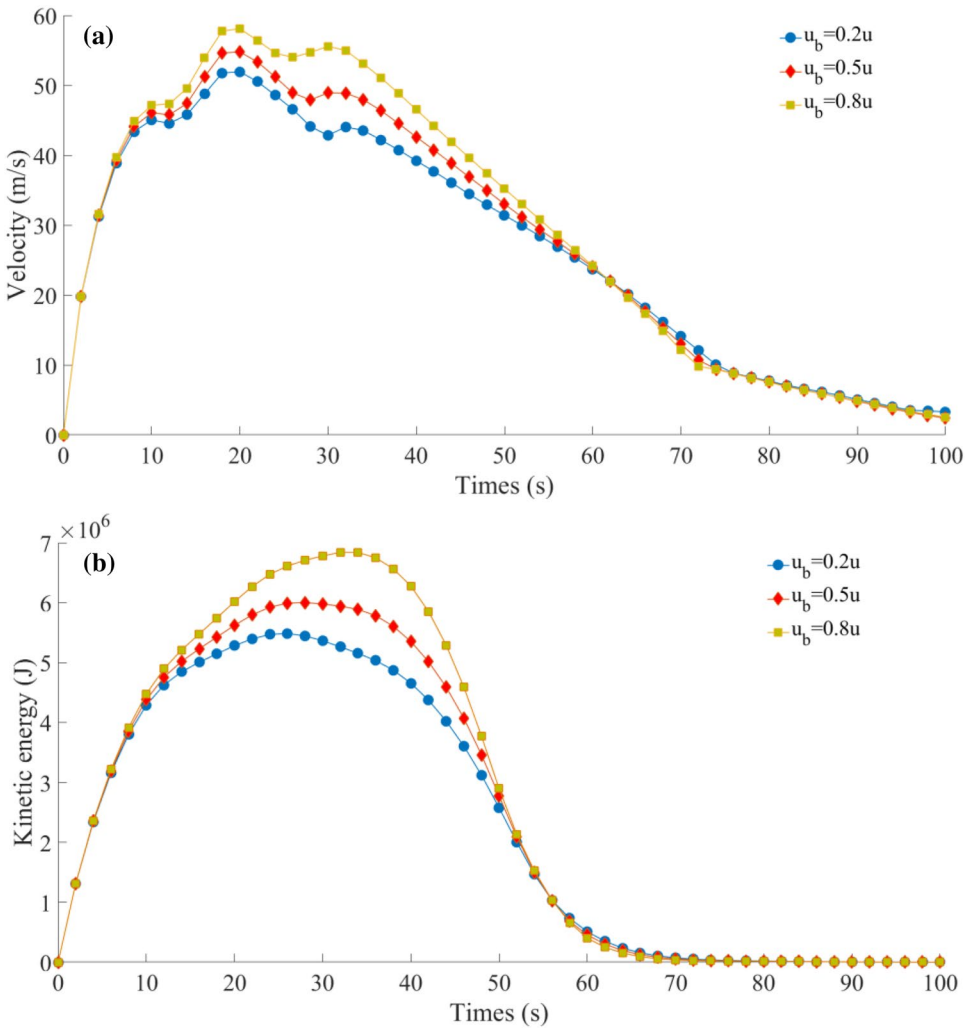

Fig. 14 Evolutions of maximum velocity and total kinetic energy of the landslide in simulations with different values of $\mathbf{u}_b$

Acknowledgements This work was supported by the National Natural Science Foundation of China (Grant nos. 41907241, 41790433), Original Innovation Program-CAS (Grant no. ZDBS-LY-DQC039), NSFC-ICIMOD (Grant no. 41661144041) and CAS "Light of West China" Program.

References

Allen SK, Cox SC, Owens IF (2011) Rock avalanches and other landslides in the central Southern Alps of New Zealand: a regional study considering possible climate change impacts. Landslides 8:33–48

Audusse E, Bouchut F, Bristeau MO, Klein R, Perthame BT (2004) A fast and stable well-balanced scheme with hydrostatic reconstruction for shallow water flows. SIAM J Sci Comput 25:2050–2065

Bai X, Jian J, He S, Liu W (2019) Dynamic process of the massive Xinmo landslide, Sichuan (China), from joint seismic signal and morphodynamic analysis. Bull Eng Geol Environ 78(5):3269–3279

Blanc T, Pastor M, Drempetic MSV, Haddad B (2011) Depth integrated modelling of fast landslide propagation. Eur J Environ Civ Eng 15:51–72

Bollermann A, Chen G, Kurganov A, Noelle S (2013) A well-balanced reconstruction of wet/dry fronts for the shallow water equations. J Sci Comput 56:267–290

Bovis MJ, Jakob M (1999) The role of debris supply conditions in predicting debris flow activity. Earth Surf Proc Land 24(11):1039–1054

Chai HJ, Liu HC, Zhang ZY (1995) Landslide dams induced by Diexi earthquake in 1933 and its environmental effect. J Geol Hazards Environ Preserv 6:7–17

Chen H, Lee CF (2003) A dynamic model for rainfall-induced landslides on natural slopes. Geomorphology 51:269–288

Chen KT, Wu JH (2018) Simulating the failure process of the Xinmo landslide using discontinuous deformation analysis. Eng Geol 239:269–281

Chigira M, Wang WN, Furuya T, Kamai T (2003) Geological causes and geomorphological precursors of the Tsaoling landslide triggered by the 1999 Chi–Chi earthquake, Taiwan. Eng Geol 68:259–273

Cui P, Zhu YY, Han YS, Chen XQ, Zhuang JQ (2009) The 12 May Wenchuan earthquake-induced landslide lakes: distribution and preliminary risk evaluation. Landslides 6:209–223

Cuomo S, Pastor M, Capobianco V, Cascini L (2016) Modelling the space-time evolution of bed entrainment for flow-like landslides. Eng Geol 212:10–20

Davies TR, McSaveney MJ (2009) The role of rock fragmentation in the motion of large landslides. Eng Geol 109:67–79

Fan X, Xu Q, Scaringi G, Dai L, Li W, Dong X, Zhu X, Pei XJ, Dai K, Havenith HB (2017a) Failure mechanism and kinematics of the deadly June 24th 2017 Xinmo landslide, Maoxian, Sichuan, China. Landslides 14:2129–2146

Fan JR, Zhang XY, Su FH, Ge YG, Tarolli P, Yang ZY, Zeng Z (2017b) Geometrical feature analysis and disaster assessment of the Xinmo landslide based on remote sensing data. J Mt Sci 14(9):1677–1688

Fischer JT, Kowalski J, Pudasaini SP (2012) Topographic curvature effects in applied avalanche modeling. Cold Reg Sci Technol 74:21–30

Gao Y, Yin Y, Li B, Feng Z, Wang W, Zhang N, Xing A (2017) Characteristics and numerical runout modeling of the heavy rainfall-induced catastrophic landslide-debris flow at Sanxicun, Dujiangyan, China, following the Wenchuan Ms 8.0 earthquake. Landslides 14:1361–1374

Gariano SL, Guzzetti F (2016) Landslides in a changing climate. Earth Sci Rev 162:227–252

Gosse L (2000) A well-balanced flux-vector splitting scheme designed for hyperbolic systems of conservation laws with source terms. Comput Math Appl 39:135–159

Gray JMNT, Edwards AN (2014) A depth-averaged μ(I)-rheology for shallow granular free-surface flows. J Fluid Mech 755:503

Hungr O, Evans SG (2004) Entrainment of debris in rock avalanches: an analysis of a long run-out mechanism. Geol Soc Am Bull 116:1240–1252

Hungr O, McDougall S (2009) Two numerical models for landslide dynamic analysis. Comput Geosci 35:978–992

Iverson RM, George DL (2015) Modelling landslide liquefaction, mobility bifurcation and the dynamics of the 2014 Oso disaster. Géotechnique 66:175–187

Iverson RM, Ouyang C (2015) Entrainment of bed material by Earth-surface mass flows: review and reformulation of depth-integrated theory. Rev Geophys 53:27–58

Khan AN, Collins AE, Qazi F (2011) Causes and extent of environmental impacts of landslide hazard in the Himalayan region: a case study of Murree, Pakistan. Nat Hazards 57:413–434

Kim SW, Chun KW, Kim JH, Kim MS, Kim MS (2012) Characteristics of heavy rainfall for landslide-triggering in 2011. J Korean For Soc 101:28–35

Legros F (2002) The mobility of long-runout landslides. Eng Geol 63:301–331

Liang Q, Borthwick AG (2009) Adaptive quadtree simulation of shallow flows with wet-dry fronts over complex topography. Comput Fluids 38:221–234

Liu W, He S, Li X, Xu Q (2016) Two-dimensional landslide dynamic simulation based on a velocity-weakening friction law. Landslides 13:957–965

Loukili Y, Soulaïmani A (2007) Numerical tracking of shallow water waves by the unstructured finite volume WAF approximation. Int J Comput Methods Eng Sci Mech 8:75–88

Lourenço SD, Sassa K, Fukuoka H (2006) Failure process and hydrologic response of a two layer physical model: implications for rainfall-induced landslides. Geomorphology 73:115–130

Mateos RM, García-Moreno I, Azañón JM (2012) Freeze–thaw cycles and rainfall as triggering factors of mass movements in a warm Mediterranean region: the case of the Tramuntana Range (Majorca, Spain). Landslides 9:417–432

McDougall S, Hungr O (2005) Dynamic modelling of entrainment in rapid landslides. Can Geotech J 42:1437–1448

Ouyang C, He S, Tang C (2015) Numerical analysis of dynamics of debris flow over erodible beds in Wenchuan earthquake-induced area. Eng Geol 194:62–72

Ouyang C, Zhou K, Xu Q, Yin J, Peng D, Wang D, Li W (2017a) Dynamic analysis and numerical modeling of the 2015 catastrophic landslide of the construction waste landfill at Guangming, Shenzhen, China. Landslides 14:705–718

Ouyang CJ, Zhao W, He SM, Wang DP, Zhou S, An HC, Wang ZW, Cheng DX (2017b) Numerical modeling and dynamic analysis of the 2017 Xinmo landslide in Maoxian County, China. J Mt Sci 14:1701–1711

Pastor M, Blanc T, Haddad B, Petrone S, Morles MS, Drempetic V, Issler D, Crosta GB, Cascini L, Sorbino G, Cuomo S (2014) Application of a SPH depth-integrated model to landslide run-out analysis. Landslides 11:793–812

Pirulli M, Pastor M (2012) Numerical study on the entrainment of bed material into rapid landslides. Geotechnique 62:959

Pitman EB, Nichita CC, Patra AK, Bauer AC, Bursik M, Weber A (2003) A model of granular flows over an erodible surface. Discrete Contin Dyn Syst Ser B 3:589–600

Pudasaini SP, Fischer JT (2016) A mechanical erosion model for two-phase mass flows. arXiv preprint arXiv:1610.01806

Pudasaini SP, Miller SA (2013) The hypermobility of huge landslides and avalanches. Eng Geol 157:124–132

Rahman AU, Khan AN, Collins AE (2014) Analysis of landslide causes and associated damages in the Kashmir Himalayas of Pakistan. Nat Hazards 71:803–821

Regmi AD, Yoshida K, Dhital MR, Devkota K (2013) Effect of rock weathering, clay mineralogy, and geological structures in the formation of large landslide, a case study from Dumre Besei landslide, Lesser Himalaya Nepal. Landslides 10:1–13

Savage SB, Hutter K (1989) The motion of a finite mass of granular material down a rough incline. J Fluid Mech 199:177–215

Su LJ, Hu KH, Zhang WF, Wang J, Lei Y, Zhang CL, Cui P, Pasuto A, Zheng QH (2017) Characteristics and triggering mechanism of Xinmo landslide on 24 June 2017 in Sichuan, China. J Mt Sci 14(9):1689–1700

Tsou CY, Feng ZY, Chigira M (2011) Catastrophic landslide induced by typhoon Morakot, Shiaolin, Taiwan. Geomorphology 127:166–178

Wang LS, Yang LZ, Li TB, Xu XN, Wang XQ, Cui J (2008) Diexi earthquake-induced landslide, Min River, Sichuan Province (1933). In: Huang RQ, Xu Q (eds) Catastrophic landslides in China. Science Press, Beijing, pp 57–93

Yin Y, Wang F, Sun P (2009) Landslide hazards triggered by the 2008 Wenchuan earthquake, Sichuan, China. Landslides 6:139–152

Yin Y, Wang W, Zhang N, Yan J, Wei Y (2017) The June 2017 Maoxian landslide: geological disaster in an earthquake area after the Wenchuan Ms 8.0 earthquake. Sci China Technol Sci 60:1762–1766

Zhou JW, Cui P, Hao MH (2016) Comprehensive analyses of the initiation and entrainment processes of the 2000 Yigong catastrophic landslide in Tibet, China. Landslides 13(1):39–54